

Article

Influence of MXene (Ti_3C_2) Phase Addition on the Microstructure and Mechanical Properties of Silicon Nitride Ceramics

Jaroslav Wozniak ^{1,*}, Mateusz Petrus ¹, Tomasz Cygan ¹, Artur Lachowski ¹,
Bogusława Adamczyk-Cieślak ¹, Dorota Moszczyńska ¹, Agnieszka Jastrzębska ¹,
Tomasz Wojciechowski ², Wanda Ziemkowska ² and Andrzej Olszyna ¹

¹ Faculty of Material Science and Engineering, Warsaw University of Technology, Wołoska 141 Str, 02-507 Warsaw, Poland; mateusz.petrus.dokt@pw.edu.pl (M.P.); tomasz.cygan.dokt@pw.edu.pl (T.C.); artur.lachowski.dokt@pw.edu.pl (A.L.); bogusława.cieslak@pw.edu.pl (B.A.-C.); dorota.moszczyńska@pw.edu.pl (D.M.); agnieszka.jastrzebska@pw.edu.pl (A.J.); andrzej.olszyna@pw.edu.pl (A.O.)

² Faculty of Chemistry, Warsaw University of Technology, Noakowskiego 3, 00-664 Warsaw, Poland; twojciechowski@ch.pw.edu.pl (T.W.); ziemk@ch.pw.edu.pl (W.Z.)

* Correspondence: jaroslav.wozniak@pw.edu.pl

Received: 16 October 2020; Accepted: 16 November 2020; Published: 19 November 2020



Abstract: This paper discusses the influence of Ti_3C_2 (MXene) addition on silicon nitride and its impact on the microstructure and mechanical properties of the latter. Composites were prepared through powder processing and sintered using the spark plasma sintering (SPS) technic. Relative density, hardness and fracture toughness, were analyzed. The highest fracture toughness at $5.3 \text{ MPa}\cdot\text{m}^{1/2}$ and the highest hardness at HV5 2217 were achieved for 0.7 and 2 wt.% Ti_3C_2 , respectively. Moreover, the formation of the $\text{Si}_2\text{N}_2\text{O}$ phase was observed as a result of both the MXene addition and the preservation of the $\alpha\text{-Si}_3\text{N}_4 \rightarrow \beta\text{-Si}_3\text{N}_4$ phase transformation during the sintering process.

Keywords: sintering; composites; mechanical properties; Si_3N_4

1. Introduction

Silicon nitride is used in many different applications thanks to its excellent mechanical properties at elevated temperatures, thermal shock resistance and good tribological and wear properties [1–4]. Silicon nitride crystallizes in two allotropic forms: low-temperature $\alpha\text{-Si}_3\text{N}_4$ and high-temperature $\beta\text{-Si}_3\text{N}_4$. Both types have a hexagonal structure but different stacking sequences: ABCD in the case of $\alpha\text{-Si}_3\text{N}_4$ and ABAB in $\beta\text{-Si}_3\text{N}_4$. This affects the properties of individual phases: $\alpha\text{-Si}_3\text{N}_4$ is characterized by higher hardness, while $\beta\text{-Si}_3\text{N}_4$ has higher chemical resistance. The transformation of α into β takes place within the temperature range of 1300 to 1800 °C. The $\alpha\text{-Si}_3\text{N}_4 \rightarrow \beta\text{-Si}_3\text{N}_4$ transformation requires the presence of a liquid phase and consists of dissolving $\alpha\text{-Si}_3\text{N}_4$ in a liquid and precipitation on the $\beta\text{-Si}_3\text{N}_4$ nuclei. The grains of the $\beta\text{-Si}_3\text{N}_4$ phase have elongated shapes and their morphology resembles whiskers [5,6]. The $\alpha\text{-Si}_3\text{N}_4 \rightarrow \beta\text{-Si}_3\text{N}_4$ transformation is a factor that facilitates densification during the sintering process. In addition to controlling the amount of the $\beta\text{-Si}_3\text{N}_4$ phase in the ceramic sinter and the texturization of the $\beta\text{-Si}_3\text{N}_4$, this transformation can be used to improve the mechanical properties of the produced Si_3N_4 ceramic [7]. The preparation of self-reinforced Si_3N_4 allows a high fracture toughness, i.e., greater than $11 \text{ MPa}\cdot\text{m}^{1/2}$, to be obtained; however, it has a negative impact on the bending strength [8,9]. A significant improvement of this parameter can be achieved by texturizing the Si_3N_4 microstructure [1]. Hirao et al. [9] produced textured $\beta\text{-Si}_3\text{N}_4$ ceramics with a fracture toughness of $11.1 \text{ MPa}\cdot\text{m}^{1/2}$ and a bending strength of 1.1 GPa. They used seeding and tape

casting methods. Teshima et al. [10] obtained high values of fracture toughness ($14 \text{ MPa}\cdot\text{m}^{1/2}$) and bending strength (1.4 GPa) for ceramics produced using seeding and extrusion. In addition to the above-mentioned methods, matrix composites can also be used to improve the properties of Si_3N_4 . Components such as TiN, SiC whiskers, ZrO_2 nanofibers and graphene can be used as reinforcing phases [11–16]. Very interesting research results have been obtained in the case of composites reinforced with graphene. Cygan et al. [2] produced Si_3N_4 -1 wt.% G/C composites using the spark plasma sintering (SPS) method. They determined the influence of the sintering temperature on the β - Si_3N_4 properties and phase content formed during the consolidation of the composites. They determined the optimal sintered temperature to be $1700 \text{ }^\circ\text{C}$, and observed a stabilization of the α - Si_3N_4 phase through the addition of graphene. Similar results have been presented by Rutkowski et al. [16]. They observed a decrease in the β - Si_3N_4 phase content with an increase of the graphene amount for composites consolidated with a hot pressing (HP) technique. In addition to the studies listed above, MXene phases have recently attracted a lot of attention. MXene phases are a large family of materials (carbides and nitrides) with two-dimensional (2D) structures. The strong covalent bonds between M–X entail high mechanical properties, making these materials potentially useful as reinforcing phases for composites. Additionally, the good conductivity and excellent volumetric capacity of these materials mean that they are commonly used in many industries, such as medicine, optoelectronics and energy storage. MXene phases are synthesized from MAX phases. They constitute a large group of anisotropic crystalline materials and their name reflects their composition, i.e., $\text{M}_{n+1}\text{AX}_n$, where M is a light transition metal, e.g., Ti, Nb, V; A is a metal from group 13 or 14; and X is carbon or nitrogen. The MAX phases exhibit a layered structure in which there is a metallic layer between M–X. In the process of synthesizing the MXene phases, this metallic layer is etched and then the products are removed in the rinsing process. In the final stage, the etched structures are delaminated into 2D structures. With regard to MXene phases, one great difficulty in using them as reinforcing phases is their thermal stability [17–19]. Depending on the conditions, the decomposition of MXene can occur at temperatures as low as $200 \text{ }^\circ\text{C}$ in an air atmosphere. In argon, the thermal stability of the MXene phases is much higher. The formation of anatase has been observed at temperatures above $800 \text{ }^\circ\text{C}$. In both cases, the MXene was completely oxidized above $1000 \text{ }^\circ\text{C}$ and rutile was the final oxidized product [20,21]. As of yet, there are no reports in the literature on the use of MXene as a reinforcing phase in Si_3N_4 matrix composites. Only the preparation processes of composites based on SiC- and Al_2O_3 -reinforced MXene have been described [22,23]. In both studies, the authors concluded that the addition of MXene improved the mechanical properties of the produced ceramics.

The use of the SPS method is extremely important with regard to limiting the MXene oxidation. Due to short heating and cooling times and the potential complete elimination of dwell time, it is possible to reduce the MXene phase decomposition, as in the case of composites reinforced with graphene [24]. For ceramic composites reinforced with graphene, it has been confirmed that the graphitization of graphene particles was reduced by using the SPS method. Moreover, a short sintering time and a lower sintering temperature also affected the properties of ceramics by limiting grain growth [25].

The main aim of this paper is to determine the effect of the addition of MXene to Si_3N_4 on the microstructure and mechanical properties of the obtained ceramics. To the best of our knowledge, this is the first study on the sintering of Si_3N_4 with the addition of MXene.

2. Materials and Methods

In the experimental work carried out to determine the effect of the addition of MXene to Si_3N_4 , the ceramics were produced using a powder metallurgy technique. α - Si_3N_4 (Grade M11, H.C. Starck, Goslar, Germany) with a chemical purity of 99.95% and average particle size of $0.6 \text{ }\mu\text{m}$ was used as a starting powder. Two sintering additives—2 wt.% MgO (Inframat Advance Materials, Manchester, CT, USA) with a chemical purity of 99.9% and average particle size of $0.3 \text{ }\mu\text{m}$ and 2 wt.% ZrO_2 (Tosoh Corporation, Tokyo, Japan) with a chemical purity of 99.8% and average particle size of $0.4 \text{ }\mu\text{m}$ —were used to

improve the consolidation of the obtained ceramics. A series of five ceramics with different additions of Ti_3C_2 -MXene (0.2, 0.5, 0.7, 1, 1.5, 2, 2.5 and 3 wt.%) were produced. Additionally, a ceramic without Ti_3C_2 , used as a reference sample, and Si_3N_4 -3 wt.% Ti_3C_2 without sintering additives were produced. Ti_3AlC_2 (MAX phase) was used as a starting material for the preparation of the MXene. It was synthesized using the SPS technique. Powdered Ti, Al and C were mixed in a ratio of 3:1:1.9 in a ball mill for 24 h. After drying and granulation, they were subjected to SPS synthesis (SPS HP D10, FCT Systeme GmbH, Effelder-Rauenstein, Germany) at a temperature of 1300 °C for 3 min under a vacuum. The material prepared in this way was then grinded. The preparation of MXene Ti_3C_2 was carried out through the acidic etching of the MAX Ti_3AlC_2 phase with concentrated (48%) hydrofluoric (HF) acid, under a fume hood. The MAX phase was slowly added to the HF, in portions, in amounts of 1 g MAX per 10 g of HF. The mixture was then stirred at 1000 rpm for 24 h until all available Al layers were removed. The resulting precipitate was separated from the acidic mixture and washed thoroughly with distilled water until the pH of the clay reached c.a. 7. The obtained Ti_3C_2 MXene was washed with ethanol, allowed to dry for 24 h at room temperature (RT) and then stored at 5 °C in the dark.

The obtained MXene powder was then subjected to the second stage of processing, in which the lamellar structure of the MXene was fragmented into single, multilayer (ML) flakes using a stepwise sonication process. This process was recently developed by the authors [26] specifically to avoid delamination into single-layered flakes, which are known to rapidly oxidize [27] and decompose in the course of the sintering process. Recent theoretical and experimental studies have shown that ML flakes are more stable compared to single-layered flakes [28]. Briefly, the first step of the sonication process was carried out in dried nonpolar hexane in a ratio of 1 g of powder to 50 cm³ of solvent for 2 h. To avoid overheating, an ice bath was used, together with a periodic working mode (1 s working, 3 s resting). The sediment was collected and dried for 2 h at RT and then subjected to sonication in dried polar isopropanol for 1 h via the same sonication procedure as in the case of hexane. After drying at RT, the 2D ML- $\text{Ti}_3\text{C}_2\text{T}_x$ flakes were stored at 5 °C in the dark.

The prepared powder mixtures were homogenized in a planetary mill for 10 h in an isopropyl alcohol suspension. As a grinding media, 2 mm diameter ZrO_2 balls were used with a powder-to-ball ratio of 1:10. The powder mixtures were dried at 50 °C for 24 h and then granulated using a #325 mesh sieve. The prepared mixtures were then consolidated using the SPS method. The sintering parameters used were as follows: temperature 1750 °C, heating/cooling rate 300 °C/min, dwell time 30 min, applied pressure 30 MPa, vacuum atmosphere 5×10^{-2} mbar and graphitic die and lining.

The properties of the obtained ceramics were measured using an Ultrapycnometer 1000 helium pycnometer (Quantachrome Instruments, Graz, Austria) for the skeletal density and a Vickers Hardness Tester (FV-700e, Future Tech, Kawasaki-City, Japan) for the Vickers hardness and fracture toughness (indentation method) under a load of 49 N. Before the density measurement, the samples were dried for 48 h at 60 °C. Hardness measurements were taken in accordance with EN ISO 6507-1:2007. A fracture toughness assessment was undertaken through measurement of crack lengths, propagating from the corners of the indentation as a result of pressing the Vickers indenter into the composite surface. The Niihara, Morena and Hasselman formulae were used to calculate K_{IC} [29]. In order to determine the mechanical properties of the ceramics, tests were carried out on three samples of a given composition, with at least 10 measurements for each sample. Microstructure observations of the ceramics, as well as the powders, were carried out using a scanning electron microscope (SEM Hitachi 5500, Hitachi, Tokyo, Japan). A transmission electron microscopy (TEM, Thermo Fisher Scientific, Hillsboro, OR, USA) specimen was prepared by mechanical grinding and subsequent Ar ion polishing at 4 keV to obtain an electron-transparent material. Observations were carried out using a TECNAI G2 F20 S-TWIN microscope operating at 200 kV. A Fischione 3000 high-angle annular dark field (HAADF) detector in scanning transmission electron microscopy (STEM) mode was used to collect images. The qualitative and quantitative phase compositions were analyzed using X-ray diffraction (XRD) (Bruker D8 ADVANCE X-ray diffractometer, Bruker Corporation, Billerica, MA, USA) with radiation $\text{Cu K}\alpha$ ($\lambda = 0.154056$ nm).

3. Results

Figure 1a,b show the morphology of the titanium carbide powder at each production stage. Figure 1a shows the Ti_3AlC_2 powder just after the synthesis and grinding process. The layered structure is visible; however, the individual layers are bonded by Al. The presence of the Ti_3AlC_2 phase was confirmed by the analysis of the phase composition, shown in Figure 2. It can be observed that the dominant component was Ti_3AlC_2 ; in addition to this phase, TiC was also formed as a result of the synthesis, and a small amount of unreacted graphite remained.

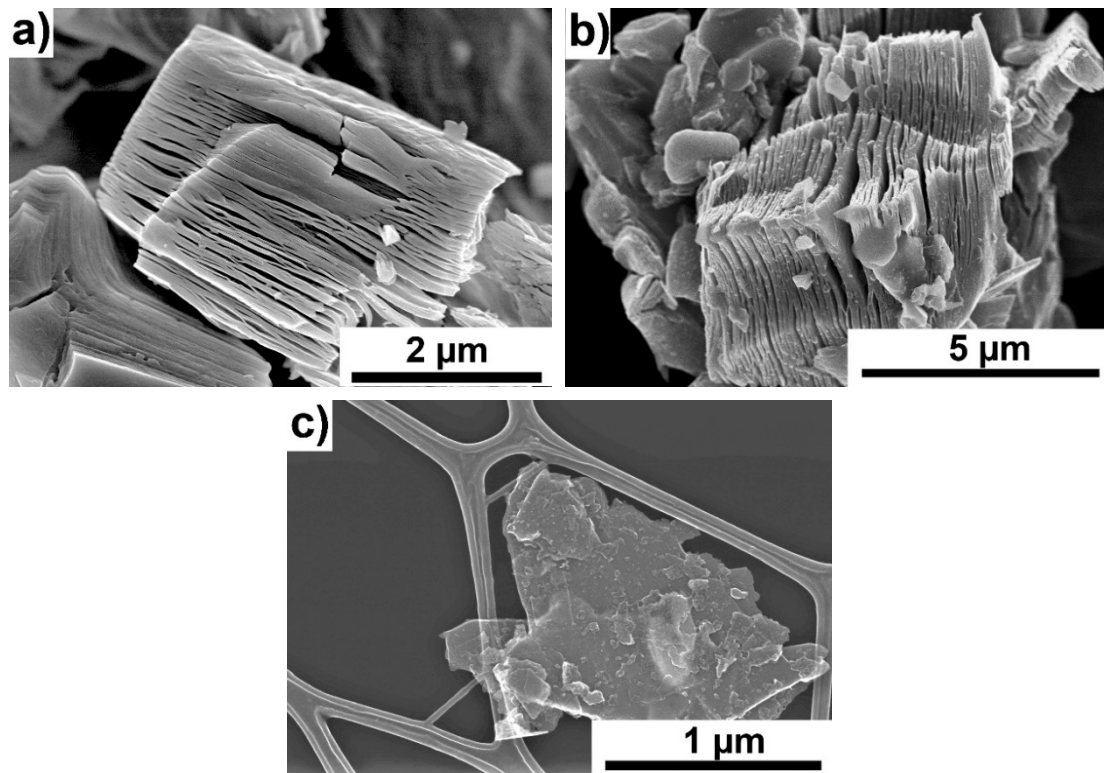


Figure 1. Morphology of Ti_3AlC_2 powder. (a) Ti_3AlC_2 MAX phases, (b) after hydrofluoric (HF) etching, (c) after delamination (Ti_3C_2 MXene).

Figure 1b shows a powder particle after HF etching. It can be seen that the Ti_3C_2 layers are separated from each other. The morphology of MXene- Ti_3C_2 is shown in Figure 1c. The particles consisting of several layers of Ti_3C_2 are visible. The prepared powders were added to Si_3N_4 in order to determine their effect on the microstructure and properties of the obtained ceramics.

Figure 3a,b show the microstructures of a pure ceramic (Figure 3a) and of a specimen with the addition of 2 wt.% Ti_3C_2 . In both cases, a fine-grained microstructure is visible. No large pores or discontinuities are visible. The presence of elongated grains of $\beta\text{-Si}_3\text{N}_4$ (marked with arrows in the figures), which were formed during the sintering process, can be observed. Moreover, it can be seen that in both the pure sample and the sample with the addition of MXene, transcrystalline fractures are the dominant fracture mechanism.

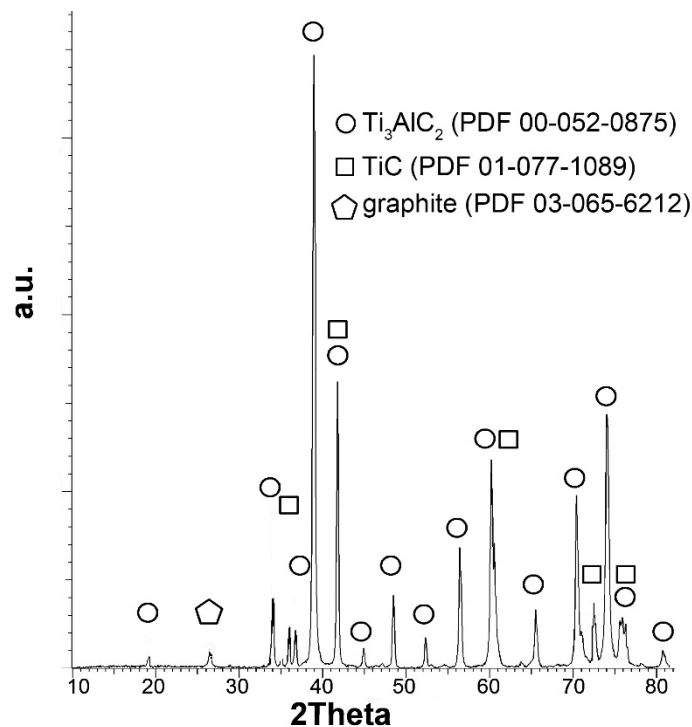


Figure 2. The X-ray diffraction (XRD) pattern obtained for synthesized Ti_3AlC_2 .

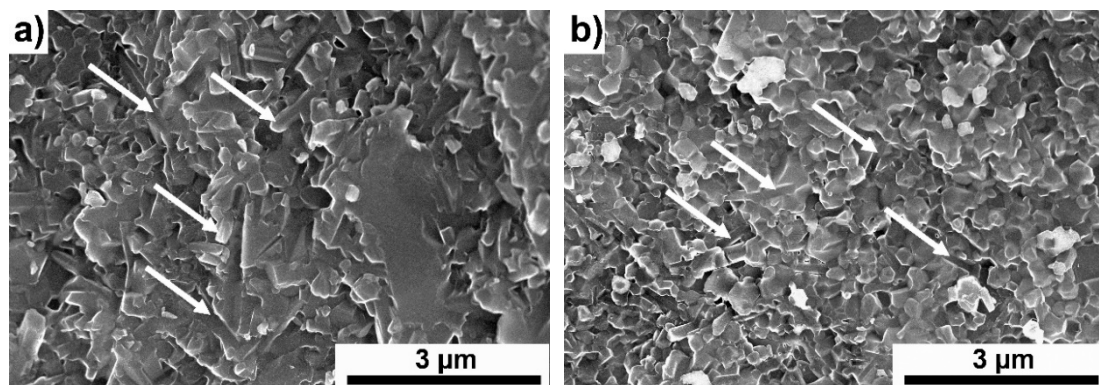


Figure 3. Fractures of (a) Si_3N_4 and (b) $\text{Si}_3\text{N}_4 + 2 \text{ wt.}\% \text{Ti}_3\text{C}_2$.

TEM analysis confirmed the observations from the scanning electron microscope. In the microstructures of the materials, both $\alpha\text{-Si}_3\text{N}_4$ and $\beta\text{-Si}_3\text{N}_4$ phases with good cohesion between individual grains (Figure 4a) are visible. Also, no pores or discontinuities can be observed. Using STEM, a third phase located on the Si_3N_4 grain boundaries was revealed (indicated by arrows in Figure 4b). The HAADF detector shows mass thickness in contrast to higher signal intensity (brightness in the image), and so this must correspond to the presence of a relatively heavy element. In this case, the only possible element was zirconium. This was confirmed by high-resolution transmission electron microscopy (HRTEM) imaging (Figure 4c).

The fast Fourier transform (FFT) pattern obtained from the region marked with the red box in Figure 4c corresponds to a monoclinic ZrO_2 phase. Again, no discontinuities in the $\text{Si}_3\text{N}_4/\text{ZrO}_2$ grain boundaries can be seen. In order to determine the influence of Ti_3C_2 addition on the sintered silicon nitride, qualitative and semiquantitative phase analyses were performed. The results of the analyses are presented in Figure 5a–c and in Table 1. With regard to the data compiled in the table, only the main phases are presented. Hence, the sum of the phases does not equal 100%. Figure 5a shows the XRD

pattern for the reference sample. It can be seen that during the sintering process, the $\alpha\text{-Si}_3\text{N}_4 \rightarrow \beta\text{-Si}_3\text{N}_4$ phase transformation took place.

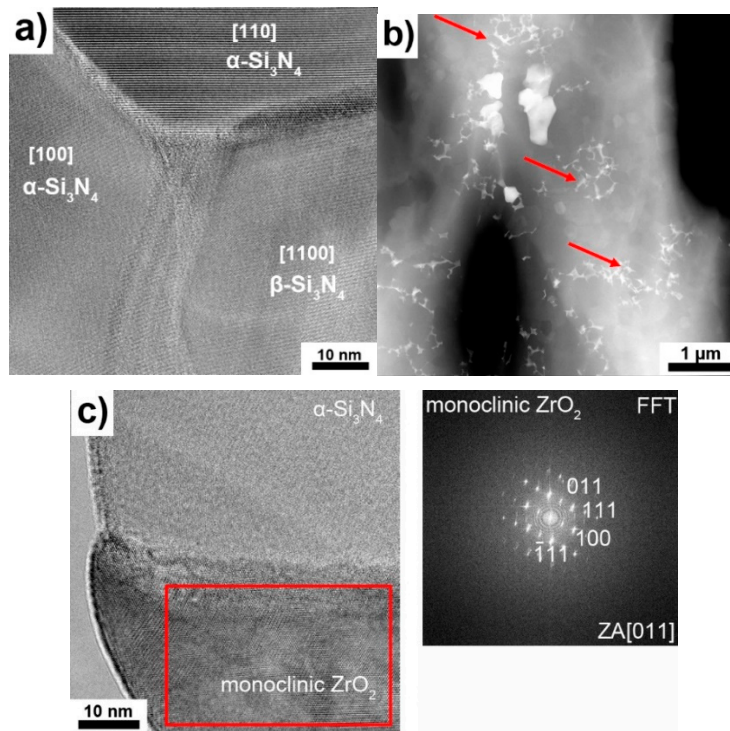


Figure 4. Transmission electron microscopy (TEM) analysis of $\text{Si}_3\text{N}_4 + 2 \text{ wt.}\% \text{Ti}_3\text{C}_2$. (a) Triple-point region of silicon nitride grains, (b) third phase located on Si_3N_4 grain boundaries, (c) high-resolution transmission electron microscopy (HRTEM) image and fast Fourier transform (FFT) pattern of third phase.

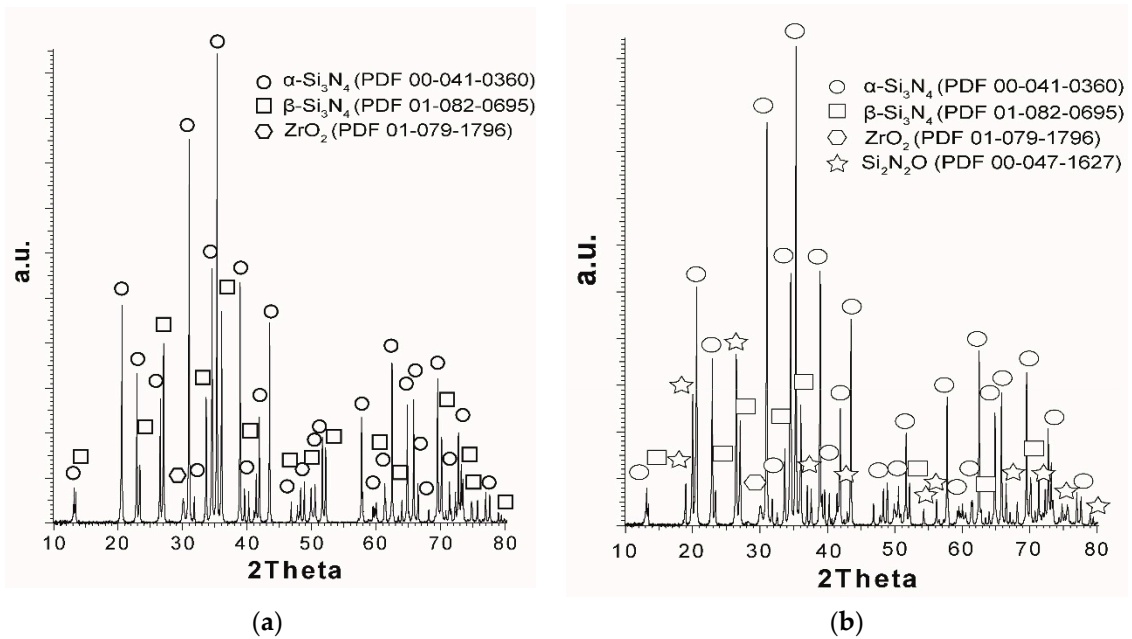
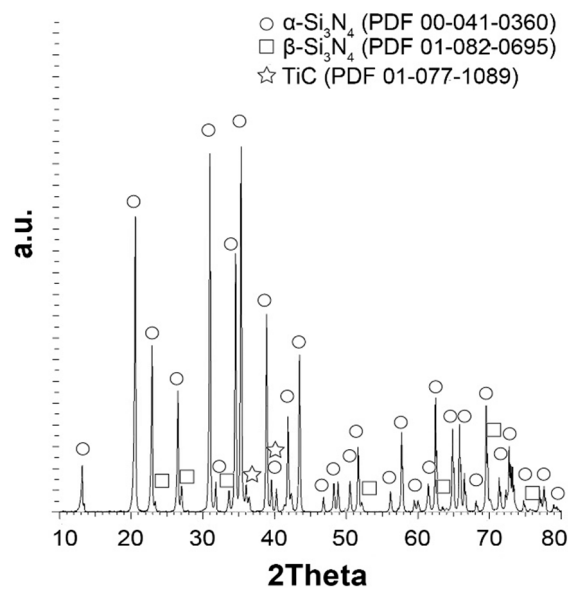


Figure 5. Cont.



(c)

Figure 5. The XRD patterns of (a) Si_3N_4 ceramics, (b) $\text{Si}_3\text{N}_4 + 3 \text{ wt.}\% \text{ Ti}_3\text{C}_2$, (c) $\text{Si}_3\text{N}_4 + 3 \text{ wt.}\% \text{ Ti}_3\text{C}_2$ (without sintering additives).

Table 1. Influence of Ti_3C_2 and sintering additive content on the α and β phase amounts in Si_3N_4 ceramics.

Sample ID	$\alpha\text{-Si}_3\text{N}_4$ [%]	$\beta\text{-Si}_3\text{N}_4$ [%]	$\text{Si}_2\text{N}_2\text{O}$ [%]
Si_3N_4	72	27	0
$\text{Si}_3\text{N}_4 + 0.7 \text{ wt.}\% \text{ Ti}_3\text{C}_2$	30	47	22
$\text{Si}_3\text{N}_4 + 2 \text{ wt.}\% \text{ Ti}_3\text{C}_2$	58	12	29
$\text{Si}_3\text{N}_4 + 3 \text{ wt.}\% \text{ Ti}_3\text{C}_2$	59	16	24
$\text{Si}_3\text{N}_4 + 3 \text{ wt.}\% \text{ Ti}_3\text{C}_2$ (without sintering additives)	94	4	0

The amount of the $\beta\text{-Si}_3\text{N}_4$ phase is estimated at 27% (Table 1). The addition of MXene to the silicon nitride significantly increased the amount of the $\beta\text{-Si}_3\text{N}_4$ phase to 47% for 0.7 wt.% Ti_3C_2 , and then decreased to 12 and 16% for 2 and 3 wt.% respectively. Moreover, in the case of the ceramics with the MXene addition, the appearance of a third $\text{Si}_2\text{N}_2\text{O}$ phase can be observed (Figure 5b). The amount only slightly changed with the Ti_3C_2 content and was about 25% (Table 1).

The formation of the $\text{Si}_2\text{N}_2\text{O}$ phase has already been described in the literature. Trigg et al. [30] proposed a reaction to form this phase in the presence of TiO_2 :



The formed SiO_2 reacts with Si_3N_4 to form $\text{Si}_2\text{N}_2\text{O}$ in the following reaction:



In the case of our ceramics, TiO_2 was not added during the powder mixing stage; however, it could form as a result of the oxidation of MXene during the sintering process. In the first stage of MXene phases oxidation, TiO_2 was produced on their surfaces, leaving behind graphene-like carbon structures [21,31]. Their presence should have favored the formation of $\text{Si}_2\text{N}_2\text{O}$ in accordance with reactions (1) and (2), but XRD phase analysis did not indicate the presence of TiN. However, the amount of this phase might have been below the detection threshold of the measurement method. Additionally, a ceramic using Ti_3C_2 without sintering activators was produced in order to determine

whether $\text{Si}_2\text{N}_2\text{O}$ phase formation is possible only in the presence of TiO_2 . On the basis of the obtained results (Figure 5c and Table 1), it can be seen that a very low level of $\beta\text{-Si}_3\text{N}_4$ content was present. This was due to the small amount of the liquid phase, which is necessary for the $\alpha\text{-Si}_3\text{N}_4 \rightarrow \beta\text{-Si}_3\text{N}_4$ transformation. The small amount of this phase is related to the SiO_2 which is present on the Si_3N_4 surface [5,6,32]. Moreover, the $\text{Si}_2\text{N}_2\text{O}$ phase was not formed. This is the opposite of what is found in the literature. Wu et al. [33] investigated the effect of TiO_2 and $\text{TiO}_2/\text{ZrO}_2/\text{Y}_2\text{O}_3$ addition to Si_3N_4 on the formation of the $\text{Si}_2\text{N}_2\text{O}$ phase. They showed that $\text{Si}_2\text{N}_2\text{O}$ does not form in ceramics with oxide sintering activators. In our case, the absence of the $\text{Si}_2\text{N}_2\text{O}$ phase may be due to a small amount or lack of TiO_2 in the structure. According to [34], a sintering process without an oxide agent may lead to changes in the oxidation process. Lotfi et al. showed that as a result of Ti_3C_2 annealing in a vacuum, Ti and C atoms were rearranged to form cubic titanium carbide (TiC). This confirms our results concerning the sintering of the sample without sintering additives. The XRD tests (Figure 5c) indicate the presence of TiC. The decrease in the $\beta\text{-Si}_3\text{N}_4$ phase content for samples with a higher amount of MXene is also very interesting. The blocking of the $\alpha\text{-Si}_3\text{N}_4 \rightarrow \beta\text{-Si}_3\text{N}_4$ transformation can be caused by the presence of carbon structures formed at the initial stage of Ti_3C_2 oxidation. The range of the oxidation temperatures and $\alpha\text{-Si}_3\text{N}_4 \rightarrow \beta\text{-Si}_3\text{N}_4$ transformations are similar. The presence of layered carbon structures may inhibit the growth of the $\beta\text{-Si}_3\text{N}_4$ phase. Similar results have been obtained for Si_3N_4 composites reinforced with graphene. The presence of carbon structures in the ceramics was not confirmed in our tests. However, to comply with the oxidation scheme of MXene available in the literature, it can be presumed that carbon structures were present in the microstructures within the range of the transformation temperature, and then completely decomposed at higher temperatures.

In the next part of the research, the sample without sintering additives was omitted because the absence of such additives would result in a low degree of sample consolidation, making it impossible to perform mechanical tests for this sample. Figure 6 shows the density measurement results for the obtained ceramics. All samples with MXene addition demonstrated a lower density compared to the reference sample. The change in density as a function of the Ti_3C_2 phase content does not show any characteristic trend. The density results oscillate around 97%.

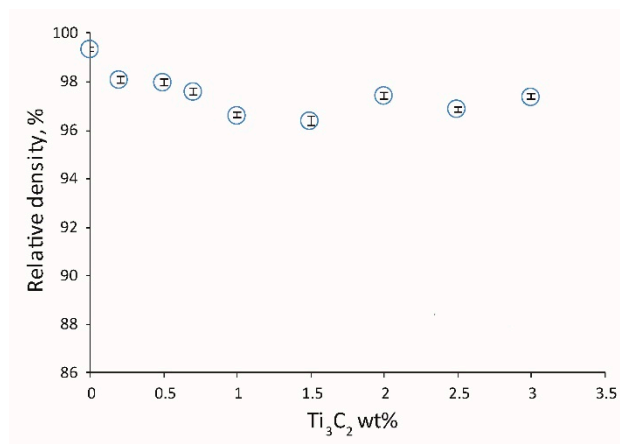


Figure 6. Influence of two-dimensional (2D) sheets of the Ti_3C_2 MXene weight content on the relative density of the composites.

Figure 7 shows the influence of the Ti_3C_2 amount on the hardness of the obtained ceramics. An increase in hardness with increasing MXene content can be seen. The highest hardness was observed for the sample with 2 wt.% Ti_3C_2 . After exceeding 2 wt.%, the hardness of the ceramic decreases. Based on the obtained results, it can be concluded that the addition of Ti_3C_2 also affects the mechanical properties of the ceramics. Despite the increase in the amount of the $\beta\text{-Si}_3\text{N}_4$ phase, in the case of lower MXene content, the hardness increases in comparison to the reference sample. Phase $\alpha\text{-Si}_3\text{N}_4$ is hard compared to phase $\beta\text{-Si}_3\text{N}_4$ [1]. Moreover, it can be seen that there is an optimal content level

for α - Si_3N_4 and β - Si_3N_4 phases for which the hardness has the highest value (the ceramic with the addition of 2 wt.% Ti_3C_2). The $\text{Si}_2\text{N}_2\text{O}$ does not have a significant effect on the ceramics' properties, since the mechanical properties of this phase are similar to those of Si_3N_4 .

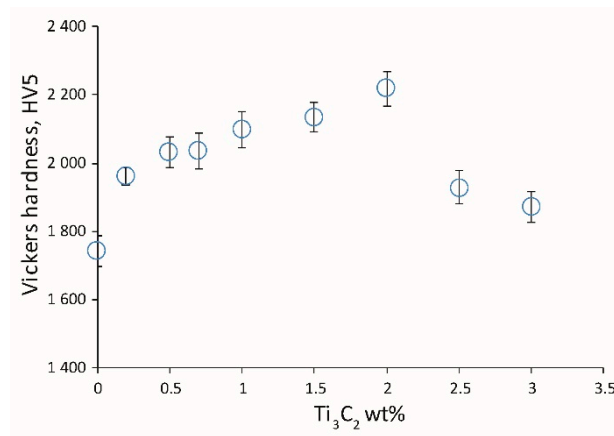


Figure 7. Influence of 2D sheets of the Ti_3C_2 MXene weight content on the Vickers hardness of the composites.

Figure 8 shows the influence of MXene content on the fracture toughness of the obtained ceramics. There is an initial increase in K_{IC} to 0.7 wt.% Ti_3C_2 , followed by a decrease. This kind of change in fracture toughness is related to the β - Si_3N_4 phase content. For higher amounts of β - Si_3N_4 phase, higher K_{IC} values are observed.

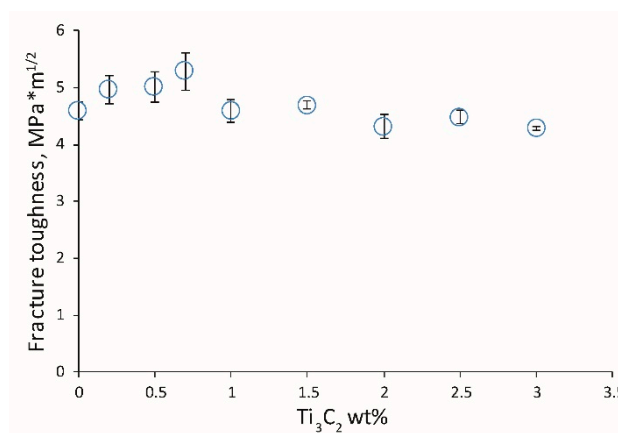


Figure 8. Influence of 2D sheets of the Ti_3C_2 MXene weight content on the fracture toughness of the composites.

4. Conclusions

In this study, research was carried out to determine the effect of MXene phase addition on the mechanical properties and microstructure of Si_3N_4 ceramics. The obtained results indicate the absence of MXene phases after the sintering process. This proves that there is no possibility of producing MXene composites reinforced with the Si_3N_4 matrix with oxide sintering activators. The addition of Ti_3C_2 , however, enables the modification of the phase composition of the ceramics by limiting the α - $\text{Si}_3\text{N}_4 \rightarrow \beta$ - Si_3N_4 phase transformation and introducing an additional $\text{Si}_2\text{N}_2\text{O}$ phase. By adding a certain amount of MXene, it is also possible to control mechanical properties such as hardness and fracture toughness.

Author Contributions: J.W.: article concept, manuscript preparation, ceramics preparation, SEM observation, results analysis, MAX preparation; M.P. and T.C.: mechanical properties tests, MAX preparation; A.L.: TEM observation; B.A.-C.: semi-quantitative phase analysis; D.M.: MAX powders XRD analysis; A.J., T.W., W.Z.: MXene preparation; A.O.: review and edition. All authors have read and agreed to the published version of the manuscript.

Funding: The study was accomplished thanks to the funds allotted by the National Science Centre within the framework of the research project ‘OPUS 13’ no. UMO-2017/25/B/ST8/01205.

Conflicts of Interest: The authors declare no conflict of interest.

References

1. Zhu, X.; Sakka, Y. Textured silicon nitride: Processing and anisotropic properties. *Sci. Technol. Adv. Mater.* **2008**, *9*. [CrossRef] [PubMed]
2. Cygan, T.; Woźniak, J.; Kostecki, M.; Cieślak, B.A.; Olszyna, A.R. Influence of graphene addition and sintering temperature on physical properties of Si₃N₄ matrix composites. *Int. J. Refract. Met. Hard Mater.* **2016**, *57*, 19–23. [CrossRef]
3. Iturriza, I.; Castro, F.; Fuentes, M. Sinter and sinter-HIP of silicon nitride ceramics with yttria and alumina additions. *J. Mater. Sci.* **1989**, *24*, 2047–2056. [CrossRef]
4. Guedes-Silva, C.C.; Carvalho, F.M.D.S.; Bressiani, J.C. Effect of rare-earth oxides on properties of silicon nitride obtained by normal sintering and sinter-HIP. *J. Rare Earths* **2012**, *30*, 1177–1183. [CrossRef]
5. Suematsu, H.; Mitomo, M.; Mitchell, T.E.; Petrovic, J.J.; Fukunaga, O.; Ohashi, N. The α - β Transformation in Silicon Nitride Single Crystals. *J. Am. Ceram. Soc.* **1997**, *80*, 615–620. [CrossRef]
6. Sarin, V. On the α -to- β phase transformation in silicon nitride. *Mater. Sci. Eng. A* **1988**, *105–106*, 151–159. [CrossRef]
7. Zhang, Z.; Duan, X.; Qiu, B.; Yang, Z.; Cai, D.; He, P.; Jia, D.; Zhou, Y. Preparation and anisotropic properties of textured structural ceramics: A review. *J. Adv. Ceram.* **2019**, *8*, 289–332. [CrossRef]
8. Kawashima, T.; Okamoto, H.; Yamamoto, H.; Kitamura, A. Grain Size Dependence of the Fracture Toughness of Silicon Nitride Ceramics. *J. Ceram. Soc. Jpn.* **1991**, *99*, 320–323. [CrossRef]
9. Hirao, K.; Nagaoka, T.; Brito, M.E.; Kanzaki, S. Microstructure Control of Silicon Nitride by Seeding with Rodlike beta-Silicon Nitride Particles. *J. Am. Ceram. Soc.* **1994**, *77*, 1857–1862. [CrossRef]
10. Teshima, H.; Hirao, K.; Toriyama, M.; Kanzaki, S. Fabrication and Mechanical Properties of Silicon Nitride Ceramics with Unidirectionally Oriented Rodlike Grains. *J. Ceram. Soc. Jpn.* **1999**, *107*, 1216–1220. [CrossRef]
11. Buljan, S.; Sarin, V. Silicon nitride-based composites. *Composites* **1987**, *18*, 99–106. [CrossRef]
12. Wang, C.-A.; Yong, H.; Hongxiang, Z. The Effect of Whisker Orientation in SiC Whisker-Reinforced Si₃N₄ Ceramic Matrix Composites. Available online: <http://www.paper.edu.cn> (accessed on 10 September 2020).
13. Ahmad, N.; Sueyoshi, H. Properties of Si₃N₄-TiN composites fabricated by spark plasma sintering by using a mixture of Si₃N₄ and Ti powders. *Ceram. Int.* **2010**, *36*, 491–496. [CrossRef]
14. Ramirez, C.; Figueiredo, F.M.; Miranzo, P.; Poza, P.; Osendi, M.I. Graphene nanoplatelet/silicon nitride composites with high electrical conductivity. *Carbon* **2012**, *50*, 3607–3615. [CrossRef]
15. Yang, Y.; Li, B.; Zhang, C.; Wang, S.; Liu, K.; Yang, B. Fabrication and properties of graphene reinforced silicon nitride composite materials. *Mater. Sci. Eng. A* **2015**, *644*, 90–95. [CrossRef]
16. Rutkowski, P.; Stobierski, L.; Górný, G. Thermal stability and conductivity of hot-pressed Si₃N₄-graphene composites. *J. Therm. Anal. Calorim.* **2014**, *116*, 321–328. [CrossRef]
17. *Advances in Science and Technology of Mn+1AX_n Phases*; Woodhead Publishing: Cambridge, UK, 2012.
18. Naguib, M.; Mashtalir, O.; Carle, J.; Presser, V.; Lu, J.; Hultman, L.; Gogotsi, Y.; Barsoum, M.W. Two-Dimensional Transition Metal Carbides. *ACS Nano* **2012**, *6*, 1322–1331. [CrossRef]
19. Eklund, P.; Rosen, J.; Persson, P.O. Å Layered ternary Mn+1AX_n phases and their 2D derivative MXene: An overview from a thin-film perspective. *J. Phys. D Appl. Phys.* **2017**, *50*, 113001. [CrossRef]
20. Wang, K.; Zhou, Y.; Xu, W.; Huang, D.; Wang, Z.; Hong, M. Fabrication and thermal stability of two-dimensional carbide Ti₃C₂ nanosheets. *Ceram. Int.* **2016**, *42*, 8419–8424. [CrossRef]
21. Li, Z.; Wang, L.; Sun, D.; Zhang, Y.; Liu, B.; Hu, Q.; Zhou, A.-G. Synthesis and thermal stability of two-dimensional carbide MXene Ti₃C₂. *Mater. Sci. Eng. B* **2015**, *191*, 33–40. [CrossRef]
22. Fei, M.; Lin, R.; Lu, Y.; Zhang, X.; Bian, R.; Cheng, J.; Luo, P.; Xu, C.; Cai, D. MXene-reinforced alumina ceramic composites. *Ceram. Int.* **2017**, *43*, 17206–17210. [CrossRef]

23. Woźniak, J.; Petrus, M.; Cygan, T.; Jastrzębska, A.; Wojciechowski, T.; Ziemkowska, W.; Olszyna, A. Silicon carbide matrix composites reinforced with two-dimensional titanium carbide—Manufacturing and properties. *Ceram. Int.* **2019**, *45*, 6624–6631. [[CrossRef](#)]
24. Inam, F.; Yan, H.; Reece, M.J.; Peijs, T. Structural and chemical stability of multiwall carbon nanotubes in sintered ceramic nanocomposite. *Adv. Appl. Ceram.* **2010**, *109*, 240–247. [[CrossRef](#)]
25. Woźniak, J.; Cygan, T.; Petrus, M.; Cygan, S.; Kostecki, M.; Jaworska, L.; Olszyna, A.R. Tribological performance of alumina matrix composites reinforced with nickel-coated graphene. *Ceram. Int.* **2018**, *44*, 9728–9732. [[CrossRef](#)]
26. Rozmysłowska, A.; Wojciechowski, T.; Ziemkowska, W.; Chlubny, L.; Olszyna, A.R.; Jastrzębska, A.M. Surface interactions between 2D Ti_3C_2/Ti_2C MXenes and lysozyme. *Appl. Surf. Sci.* **2019**, *473*, 409–418. [[CrossRef](#)]
27. Jastrzębska, A.M.; Szuplewska, A.; Rozmysłowska-Wojciechowska, A.; Chudy, M.; Olszyna, A.; Birowska, M.; Popielski, M.; Majewski, J.A.; Scheibe, B.; Natu, V.; et al. On tuning the cytotoxicity of Ti_3C_2 (MXene) flakes to cancerous and benign cells by post-delamination surface modifications. *2D Mater.* **2020**, *7*, 025018. [[CrossRef](#)]
28. Szuplewska, A.; Rozmysłowska-Wojciechowska, A.; Poźniak, S.; Wojciechowski, T.; Birowska, M.; Popielski, M.; Chudy, M.; Ziemkowska, W.; Chlubny, L.; Moszczyńska, D.; et al. Multilayered sTable 2D nano-sheets of Ti_2NT_x MXene: Synthesis, characterization, and anticancer activity. *J. Nanobiotechnol.* **2019**, *17*, 114. [[CrossRef](#)]
29. Ponton, C.B.; Rawlings, R.D. Vickers indentation fracture toughness test Part 1 Review of literature and formulation of standardised indentation toughness equations. *Mater. Sci. Technol.* **1989**, *5*, 865–872. [[CrossRef](#)]
30. Trigg, M.B.; McCartney, E.R. Comparison of the Reaction Systems $ZrO_2-Si_3N_4$ and $TiO_2-Si_3N_4$. *J. Am. Ceram. Soc.* **1981**, *64*, C-151–C-152. [[CrossRef](#)]
31. Naguib, M.; Mashtalir, O.; Lukatskaya, M.R.; Dyatkin, B.; Zhang, C.; Presser, V.; Gogotsi, Y.; Barsoum, M.W. One-step synthesis of nanocrystalline transition metal oxides on thin sheets of disordered graphitic carbon by oxidation of MXenes. *Chem. Commun.* **2014**, *50*, 7420–7423. [[CrossRef](#)]
32. Riley, F.L. Silicon Nitride and Related Materials. *J. Am. Ceram. Soc.* **2000**, *83*, 245–265. [[CrossRef](#)]
33. Wu, L.-X.; Guo, W.-M.; Zeng, L.-Y.; Lin, H.-T. Equiaxed $\beta-Si_3N_4$ ceramics prepared by rapid reaction-bonding and post-sintering using $TiO_2-Y_2O_3-Al_2O_3$ additives. *J. Am. Ceram. Soc.* **2017**, *100*, 5353–5357. [[CrossRef](#)]
34. Lotfi, R.; Naguib, M.; Yilmaz, D.E.; Nanda, J.; Van Duin, A.C.T. A comparative study on the oxidation of two-dimensional Ti_3C_2 MXene structures in different environments. *J. Mater. Chem. A* **2018**. [[CrossRef](#)]

Publisher’s Note: MDPI stays neutral with regard to jurisdictional claims in published maps and institutional affiliations.



© 2020 by the authors. Licensee MDPI, Basel, Switzerland. This article is an open access article distributed under the terms and conditions of the Creative Commons Attribution (CC BY) license (<http://creativecommons.org/licenses/by/4.0/>).